Supplementary Materials for

Investigation on Thermodynamic Mechanisms of Brine Evaporation in Air-Carried Evaporating Separation Cycle Coupling with Process-Heat-Supplied (PHS)

Jing Yu[*a], Yujiang Xia [a], Pengfei Wang [a], Liang Chen [b] Juan Yang [a],

Changling Wang [a], Weidong Yan [a], Baobin Liu [a], Sumin Jin [c]

a: School of Internet of Things and Intelligent Engineering, Jiangsu Vocational Institute of Commerce, NO. 180 Longmian Avenue, Jiangning District, Nanjing, 211168, China

b: Yancheng Institute of Technology, NO. 1 Hope Avenue Middle Road, Yancheng, 224051, China

c: School of Energy Science and Engineering, Nanjing Tech University, NO.30 Puzhu Road(S), Nanjing, 211800, China

1 The difference between the brine atomization unit and the milk atomization unit

(a)

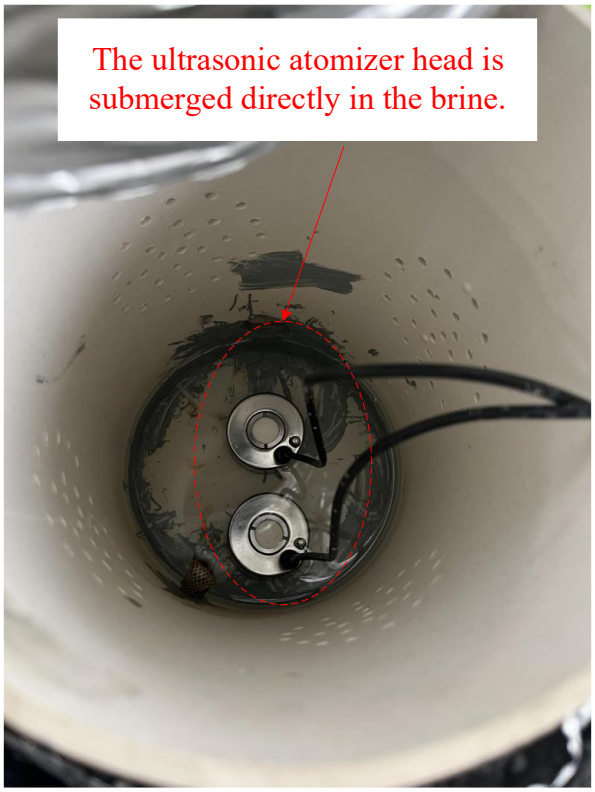

(b)

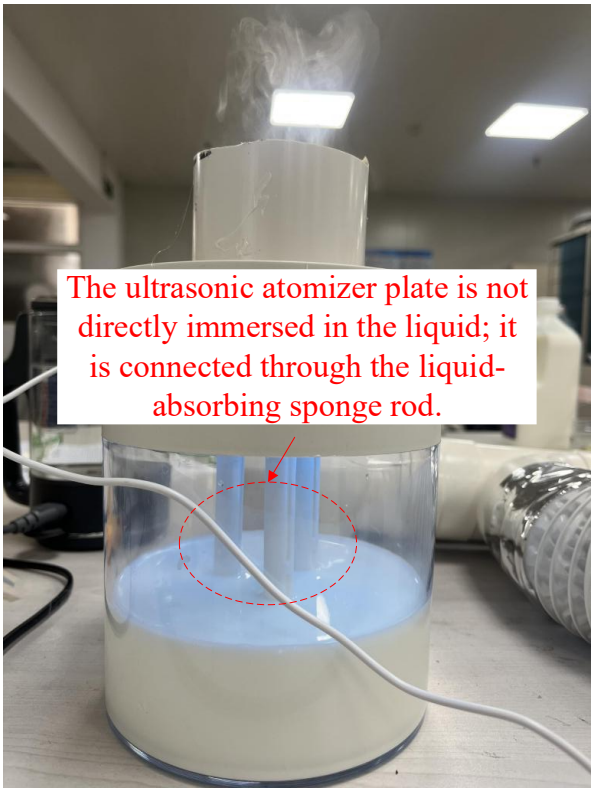

Supplementary Materials Fig.1 Comparison photograph of the brine atomization unit (a) and the milk atomization unit (b)

In the main part of the paper, through further analysis of thermodynamic mechanisms, it is demonstrated that the process-heat-supplied effect is universal. To further expand the scope of application of PHS-coupled evaporating separation technology, experiments on the evaporation and separation of milk under PHS conditions are conducted using the experimental setup shown in Fig. 1a, as described in the main text of the paper.

However, during actual experiments, we found that milk did not atomize effectively when added into the brine atomization unit. This is because the brine atomization unit is equipped with an immersion-type ultrasonic atomizer. The ultrasonic atomizer probe is directly immersed in the saline solution as shown in Supplementary Materials Fig. 1a. The ultrasonic vibrating plate generates

ultrasonic waves through high-frequency vibrations, which then pass through the liquid, causing the vibrational force to overcome the liquid surface tension and atomize the saline solution into small droplets. Nevertheless, the viscosity and surface tension of milk are significantly higher than those of brine, which is why this type of ultrasonic atomizer fails to atomize the liquid. While increasing the vibration frequency of the ultrasonic atomizer is a viable solution, it can shorten the lifespan of the atomizer.

Regarding the characteristics of milk atomization, we selected a contact-type ultrasonic atomizer. In this type of atomizer, the atomizing plate is mounted directly above a sponge or absorbent swab, ensuring that the plate does not come into direct contact with the milk. When powered on, high-frequency vibrations are transmitted through the sponge or absorbent swab to the milk in the gap, forcing the liquid through the mesh holes of the ultrasonic atomizing plate above to form droplets. With this atomization unit, milk can be effectively atomized as shown in Supplementary Materials Fig. 1b. In addition to effectively atomizing high-viscosity, high-surface-tension liquids, this type of atomization unit also reduces the risk of thermal degradation caused by localized heating, making it particularly suitable for atomizing protein-containing organic solutions. Independent operation videos for these two atomization units can be found in the Supplementary Video 5 and Supplementary Video 6.

As concluded in the main body in this paper, the final experimental results demonstrate that the employed milk atomization unit can effectively match the process-heat-supplied of the evaporating separation unit, achieving complete drying and separation of the milk at 45.23°C. The milk powder collected at the outlet can also be redissolved into milky-white milk as shown in Supplementary Video 7. This further confirms that the PHS effect is indeed universal and is not limited to the field of

separation and recovery of inorganic saline wastewater.

2 Comparative analysis of the novel simulation model with the previous model

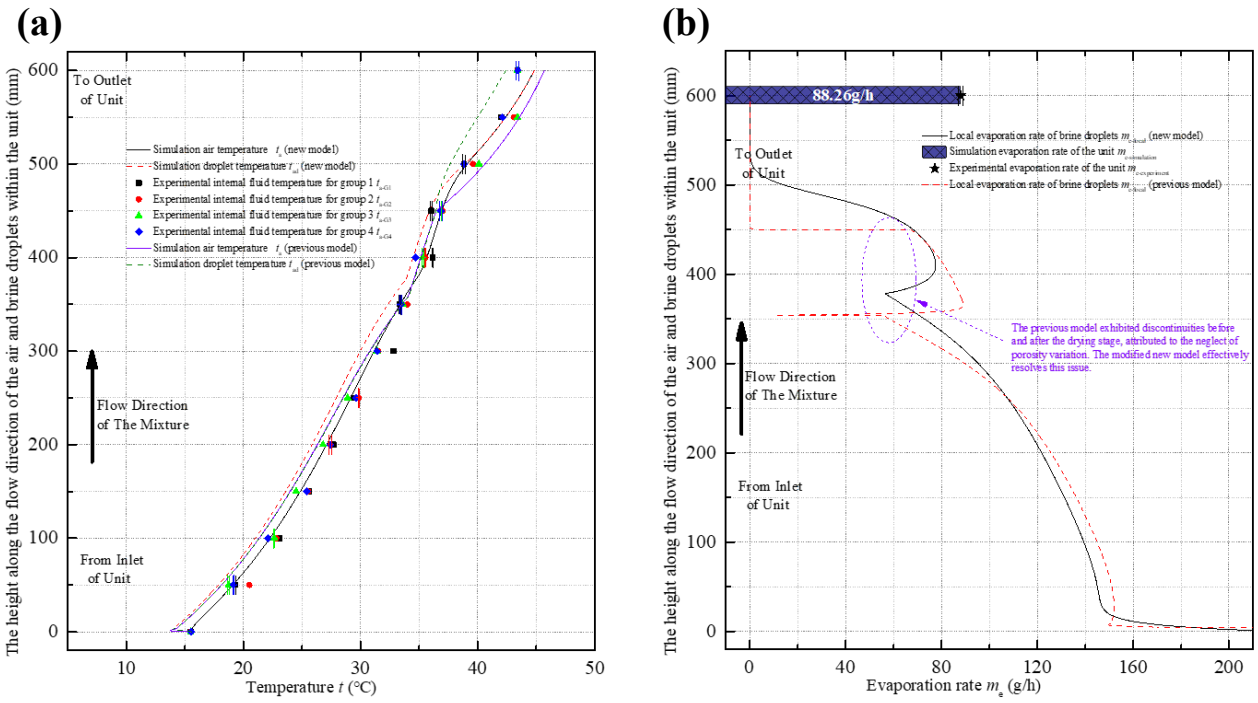

Supplementary Materials Fig.2 Comparison of calculation results between the simulation models from previous research and the modified simulation model in this work (Factor analysis operating conditions group, with ambient air as the inlet air c_{inlet}=5 %wt, $t_{a\text{-}inlet}$=15.5℃, $RH_{a\text{-}inlet}$=60.7 %) (a: Comparison of temperature variation; b: Comparison of variations in local evaporation rate)

Within the simulation method described in the main body, this investigation incorporated several model adjustments based on the newly designed PHS evaporating separation unit structure. The most significant adjustment incorporated variations in the porosity of the solid salt shell on the droplet surface into the droplet evaporation model during the drying stage. From the perspective of the overall evaporation process, as in previous research [1], using an average porosity does not lead to substantial computational errors. However, an average porosity can cause abrupt changes in the calculated local evaporation rates at the boundaries between stages ss shown in Supplementary Materials Fig.2b. In addition, as shown in Supplementary Materials Fig.2a, there is little difference in the internal

temperature profiles between the previous model and the new model. Yet a comparison reveals that the new model aligns more closely with experimental data, while the previous model yields slightly lower temperatures, indicating that slightly more energy is allocated to evaporation. This discrepancy arises precisely from the use of an average porosity. In addition, adjustments to the model based on new structural configurations (such as modifications to the equivalent diameter) can also cause deviations in the inlet effect of the device. These structural adjustments, nonetheless, have little impact on variations in local evaporation rates and temperatures. In general, whether based on experimental validation or inferences from comparative simulation analyses, it is clear that the novel model provides greater accuracy.

If we consider only the overall system, namely the inlet and outlet state parameters and the base energy efficiency, the previous simulation model is sufficient. But as this study investigates the thermodynamic mechanisms of the PHS effect, it requires a more precise simulation of the details of the internal processes. Consequently, this paper employs an updated, novel model. By combining this with subsequent entropy analysis and Gibbs free energy analysis based on the second law of thermodynamics, we have ultimately provided a comprehensive investigation of the thermodynamic mechanisms underlying this novel process.

3 Independence analysis of the simulation model

Although the control equations, structural model, and entropy equations have been updated accordingly, the basic building blocks of the simulation model in this paper still consist of control elements. Accordingly, the validation of the updated simulation model must also eliminate the influence of the number of control elements N on the simulation results. As shown in the Supply Materials Table 1 below, these are the calculated results for the primary outlet parameters of different

numbers of micro-element control volumes under factor analysis conditions and at three different supply heat water temperatures. The results indicate that when *N* reaches 60,000, the calculated values for all outlet parameters remain essentially unchanged. This means that the calculation results have converged to a specific value at this point; in other words, *N* no longer affects the simulation results, and the number of micro-element control volumes *N*, is independent of the other parameters in the model. Naturally, increasing *N* further would improve reliability, but it would also significantly increase computation time. Therefore, the choice of *N*=60,000 in this paper provides sufficient reliability.

Supply Materials Table 1 Comparison of several important outlet parameters of the unit for different Values for the micro-element control body under factor analysis conditions

Outlet supply heat water temperature (℃)	**Values for the micro-element control body *N* (-)**	**Outlet air temperature of the unit $t_{a,out}$ (℃)**	**Outlet air humidity of the unit $w_{a,out}$ (g/kg dry air)**	**Outlet droplet mass concentration $c_{ad,out}$ (wt%)**	**Time consumed to complete the simulation solution (s)**
41.23	600	35.41	24.16	27.18	22
	3000	33.76	25.02	27.32	114
	6000	34.02	24.81	27.29	235
	30000	33.99	24.84	27.29	1195
	60000	33.99	24.84	27.29	2408
51.00	600	45.89	28.64	100	21
	3000	43.61	28.64	100	112
	6000	44.92	28.64	100	227
	30000	44.83	28.64	100	1184
	60000	44.83	28.64	100	2388
61.80	600	59.15	27.77	100	21
	3000	57.33	27.77	100	110
	6000	58.07	27.77	100	224
	30000	58.04	27.77	100	1177
	60000	58.04	27.77	100	2371

3 Experimental error analysis

Analysis of experimental errors must initially evaluate the errors introduced by instruments during the measurement process. As shown in the Supply Materials Table 2, this is a summary of the models, ranges, and accuracies of all measurement instruments utilized in this experimental system. Since the air flow rate in this experiment is relatively low and it is also necessary to measure the internal temperature of the measurement unit, higher-precision ultrasonic air flow meters and thin-film thermocouples are selected accordingly. As a whole, all measurement instruments in this experimental system are highly accurate, ensuring that the experimental data readings are reliable.

Supply Materials Table 2 Types and errors of measuring instruments in this experimental system

Measuring parameter	**Measurement points**	**Measuring instrument**	**Range**	**Accuracy**
Air temperature	a0, a1, a2	High-precision temperature and humidity sensor: SHT45 - WM102	-40~120 ℃	±0.2 ℃
Air relative humidity	a0, a1, a2	High-precision temperature and humidity sensor: SHT45 - WM102	0~99.9% RH	±1 % RH
Brine temperature	w1	4-wire PT100 platinum resistance thermometer: WZP-101	-50~200 ℃	Level A: ±(0.15+0.002|t|) ℃
Supply hot water temperature	Inlet and outlet of the supply hot-water tank	4-wire PT100 platinum resistance thermometer: WZP-101	-50~200 ℃	Level A: ±(0.15+0.002|t|) ℃
Internal temperature inside the unit	4 Group, in1~in11	Surface-mount Type K Thin-Film Thermocouple: CGY-ZT-K-CZ	-40~260 ℃	±0.1 ℃
Air flow rate	a1	High-precision ultrasonic micro-flow gas flow meter: CMF-8008	0~100 L/min	±0.2% FS
Brine flow rate	w1	High-precision electronic balance: ZZ-05 (combined with a chronograph)	0~50 kg	±0.5 mL
Brine density	w1	Archimedes drainage method liquid densitometer: KW-300FG	0.0001~99.999 g/cm^3	±0.0001 g/cm^3
Power ratings of	All power components and	Digital high-precision	3.0 V~600	±0.4%×Dis

blower, pump, and heater	heaters	electric power meter: UTE9901	V 5 mA~20 A	play data +0.1%×Range

Besides the measurement errors of the instruments mentioned above, since the experimental study in this paper involves factor analysis and thermal performance research, it is imperative to conduct an uncertainty-based error analysis on all test data. A comprehensive investigation of systematic errors in the experiments is necessary to verify the reliability of the results. All experimental data covered in this paper were analyzed using a measurement error analysis method based on error propagation [3].

All parameters in this experimental investigation can be broadly classified into two categories: direct parameters (such as state parameters) and indirect parameters (such as energy efficiency parameters). The errors in direct parameters can be directly obtained from the instrument models and accuracies listed in Supply Materials Table 2, while the errors in indirect parameters were calculated using the error propagation method, as detailed below:

$$u_f = \sqrt{\sum_{i=1}^{n} \left(\frac{\partial f}{\partial x_i} u_{x_i} \right)^2} \tag{1}$$

Additionally, the relative errors of all parameters can be calculated through the method [4] in the following equation:

$$\varepsilon_x = \frac{u_x}{x_{\text{ture}}} \tag{2}$$

Supply Information Table 3 Uncertainty analysis result of the experiment

Parameter type	**Testing parameters**	**Maximum uncertainty**	**Maximum relative uncertainty**
Direct parameters	Brine temperature	±0.22 ℃	2.06 %
	Air temperature	± 0.2 ℃	3.98 %
	Air relative humidity	±1 %	4.13 %
	Supply hot water temperature	±0.29 ℃	0.66 %
	Internal temperature	±0.1 ℃	0.74 %
	Air flow rate	±0.1 L/min	2 %

	Brine flow rate	±0.032 L/min	0.5 %
	Brine density	±0.1 kg/m^3	0.001 %
	Brine mass	±0.01 g	0.00087 %
	Current	±0.01 A	2.31 %
	Voltage	±0.367 V	1.14 %
Indirect parameters	Air humidity	±0.00011 kg/kg dry air	4.26 %
	Air mass flow rate	±0.053 kg/h	2.61 %
	Brine mass flow rate	±1.73 g/h	2.02 %
	Evaporation rate	±0.0042 kg/h	3.93 %
	Evaporation efficiency	±3.38 %	4.22 %
	Exergy efficiency	±3.55 %	4.45 %
	System overall efficiency	±2.98 %	3.83 %

By calculating the errors, the maximum uncertainties of all the main parameters measured in this paper's experiments are presented in Supply Information Table 3. The maximum relative uncertainty of the indirect parameters becomes slightly higher than the maximum relative uncertainty of the direct parameters due to error propagation. Nevertheless, the maximum relative uncertainties of all parameters are less than ±5%, so it can be considered that the experimental tests in this paper are reliable and accurate.

5 Reference

[1] Yu, J., Xia, Y., Chen, L. et al. Full recovery of brines at normal temperature with process-heat-supplied coupled air-carried evaporating separation (ACES) cycle. NPJ Clean Water, 2024, 7: 133.

[2] Slezak, Andrew, Kuhlman, John M, Shadle, Lawrence J, Spenik, James, Shi, Shaoping. CFD simulation of entrained-flow coal gasification: Coal particle density/size fraction effects. Powder technology, 2010, 203: 98-108.

[3] Moffat R.J., Describing the uncertainties in experimental results. Experimental Thermal and Fluid Science, 1988, 1: 3-17.

[4] J. Osman, An Introduction to Error Analysis: The Study of Uncertainties in Physical Measurements: Second Edition. 1999, 40: 438.

6 Legend for other supplementary items

Supplementary Source Code 1 - Experimental Data Processing (Including Experimental System Performance Efficiency)

Supplementary Source Code 2 - Simulation of the Internal Thermodynamic Processes in PHS Evaporating Separation Unit (Including Entropy and Gibbs Free Energy)

Supplementary Source Code 1 PDF - Experimental Data Processing (Including Experimental System Performance Efficiency)

Supplementary Source Code 2 PDF - Simulation of the Internal Thermodynamic Processes in PHS Evaporating Separation Unit (Including Entropy and Gibbs Free Energy)

Supplementary Table 1- Original Experimental Data

Supplementary Table 2- Summary of Processed Experimental Data (Including Performance Parameters)

Supplementary Table 3- Data in figures

Supplementary Video 1 - Operational Status of the Experimental System

Supplementary Video 2 - Flow characteristics of dry salt powder dust at the outlet of the unit

Supplementary Video 3 - Salt powder adhering to the surface of the thermocouple lead sheath at the outlet

Supplementary Video 4 - Demonstration of the Independent Operation of a Brine Bubble Humidifier

Supplementary Video 5 - Demonstration of the Brine Atomization Unit in Operation

Supplementary Video 6 - Demonstration of the Milk Atomization Unit Operating Independently

Supplementary Video 7 - The collected dried milk powder can be dissolved again